Hindawi
Journal of Chemistry
Volume 2020, Article ID 8702745, 10 pages
https://doi.org/10.1155/2020/8702745

Research Article

Removal of Mercury from Coal-Fired Flue Gas and Its Sulfur Tolerance Characteristics by Mn, Ce Modified γ-Al_2O_3 Catalyst

Zhong He, Yating Xie, Yuan Wang, Jingjie Xu, and Jiangjun Hu

School of Resource and Environmental Sciences, Wuhan University, Wuhan, Hubei 430079, China

Correspondence should be addressed to Jiangjun Hu; jjhu1963@outlook.com

Received 3 April 2020; Revised 12 June 2020; Accepted 23 June 2020; Published 3 August 2020

Academic Editor: Woojin Lee

Mercury pollution in the atmospheric environment is a matter of international concern. Mercury in coal-fired flue gas is the first human mercury emission source and has become the focus of national mercury pollution control. The catalytic performance of zerovalent mercury (Hg^0) in coal-fired flue gas was studied by using manganese-cerium-aluminum oxide as catalyst. The effects of metal loading ratio, reaction temperature, calcination temperature, and O_2 and SO_2 concentration on the efficiency of Hg^0 catalytic removal were investigated, and the Mn-Ce/γ-Al_2O_3 catalysts before and after the reaction were characterized by BET, SEM, XRD, and XPS to analyze the physicochemical properties of the samples. The results show that the mercury removal efficiency of the composite catalyst with Mn, Ce, and Al as the active component is higher than that of the single metal catalyst. The catalytic activity of $Mn_{0.1}Ce_{0.02}Al$ is the best, the optimum reaction temperature is 150°C, the optimum calcination temperature is 400°C, and the O_2 concentration in the conventional flue gas condition satisfies the effective oxidation of Hg^0; SO_2 in the flue gas can seriously inhibit the oxidation of Hg^0.

1. Introduction

In China, the dominated energy structure is still coal currently [1]. Mercury emissions from coal-fired flue gas have become the largest source of mercury pollution [2]. Generally, mercury in flue gas takes on three kinds of forms: elemental mercury (Hg^0), oxidized mercury (Hg^{2+}), and particle-associated mercury (Hg^p) [3, 4]. However, Hg^0 is hard to be captured by the wet desulphurization and particulate matter control devices owing to its high volatility and low solubility in water. Thus, it makes sense to study catalysts capable of effectively transforming Hg^0 into easily captured Hg^{2+} [5, 6].

At present, the Hg^0 removal is concentrated on the modification of adsorbents and the development of new catalysts. However, the conventional SCR catalysts are not effective enough for Hg^0 oxidation in the absence of HCl [5, 7, 8]. In order to increase Hg^0 oxidation efficiency, the presence of an oxidant is generally necessary for metal oxide catalysts. Previous researches have established that chlorine is the most effective oxidant for heterogeneous mercury oxidation together with O_2 and the chlorine is originated from the HCl content in flue gas via a Deacon reaction [8–10]. However, the chlorine content of Chinese raw coal (63–318 mg/kg) is much lower than that of US coal (628 mg/kg) [11].

Transition metal oxides have a lower cost than precious metals, and their catalytic oxidation of Hg^0 has been extensively studied. Common catalyst active components include MnO_2, CuO, Co_3O_4, Fe_2O_3, CeO_2, and Cr_2O_3 [12–20]. There are many different kinds of manganese oxides and many redox reactions can use them as the electron acceptor. It is the most catalytic metal oxide in nature [21]. CeO_2 can promote the transformation of Hg^0 into oxidized Mercury even under anaerobic conditions [22, 23]. CeO_2 is a better cocatalyst, which has a good effect on the dispersion of metal active components; it can also enhance the thermal stability of the catalyst and inhibit the sintering; at the same time, CeO_2 can be effectively stored by mutual conversion between different valence states. Oxygen is collected to improve its oxidation performance [14, 24]. CeO_2 mainly

produces high activity, unstable oxygen vacancies, and bulk oxygen in the redox reaction through the mutual conversion of Ce^{3+}/Ce^{4+} [25–28]. Therefore, in low oxygen or even no oxygen, CeO_2 can also effectively promote the conversion of elemental mercury to oxidized mercury [28–31].

In this study, γ-Al_2O_3 was used as a carrier to prepare Mn-Ce-Al composite catalyst, and the performance of catalytic oxidation of Hg^0 was studied in the simulated flue gas. The effects of metal loading, calcination temperature, and reaction conditions (flue gas temperature, O_2, SO_2 concentration, etc.) on the catalytic Hg^0 removal efficiency were investigated experimentally.

2. Experimental

2.1. Catalyst Synthesis

2.1.1. Preparation of γ-Al_2O_3. 15 g of aluminum nitrate was dissolved in 100 ml of deionized water, the pH was adjusted to 10 with diluted ammonia water (volume ratio of 1 to 2), water bath for 30 minutes at 60°C, static precipitation for 2 days, filtration, drying at 105C for one night, after γ-Al_2O_3 was obtained by burning at 550°C for 1 h in an air atmosphere in a muffle furnace [32].

2.1.2. Preparation of Mn_xCe_yAl Catalyst. The obtained γ-Al_2O_3 was ground, rinsed, and dried at 90°C for 24 hours in an electric blast drying oven. Prepare a mixed solution of $C_4H_6MnO_4{\cdot}4H_2O$(AR) and $Ce(NO_3)_3{\cdot}6H_2O$(AR), then place the mixed solution on a stirrer, and slowly pour a solution containing a certain amount of γ-Al_2O_3 added dropwise with diluted aqueous ammonia to adjust the pH at 10. Precipitate the liquid for two hours at 60°C, collect the precipitate, wash with distilled water, dry overnight at 110°C, and then calcine it in air at 450°C for 4 hours. The granules were sieved with a 60–80 mesh sieve to obtain a composite catalyst of different loadings. The obtained catalyst was represented by Mn_xCe_yAl [33].

2.2. Catalytic Activity Test. As shown in Figure 1, the laboratory-scale fixed-bed system for the removal of Hg^0 and NO is composed of a gas distribution system, a mercury permeation tube (Beijing, Mingnick Analytical Instrument Equipment Center), a catalytic reactor, a temperature control system, a mercury absorption device, and an exhaust gas purification device. The catalytic reactor is placed in a temperature-programmed tubular electric furnace, and the prepared catalyst is placed in a quartz glass tube (inner diameter 10 mm, length 1000 mm). The Na_2S solution is used to absorb the mercury vapor in the exhaust gas [34], and the NaOH solution is used to absorb the acid gas in the exhaust gas.

500 mg catalyst was placed in the apparatus (the prepared catalyst was fired at 573 K for 1 h to remove moisture and other impurities). The simulated flue gas composition includes SO_2, NO, O_2, and H_2O, and the carrier gas is N_2, and the mercury vapor is carried into the pipeline and the adsorption system by the carrier gas. The mercury permeate tube is oil-bathed at 333 K. The Hg^0 concentration in the system was controlled at $55 \pm 2\,\mu g/m^3$. The gas flow rate through the reactor was 1000 mL/min (corresponding to a space velocity of 100,000 h^{-1} under standard temperature and pressure conditions). The Hg^0 concentration at the inlet and outlet of the reactor was obtained from an Hg^0 analyzer (AFS-930, Beijing Titan Instruments Co., Ltd.) [34].

2.3. Catalyst Characterization. BET (Brunauer–Emmett–Teller) is the most commonly used method for determining the specific surface area with an ASAP2020 analyzer (Micromeritics Inc., USA) at liquid nitrogen temperature. It is based on the adsorption theory, assuming the multimolecular layer adsorption occurs, and the total adsorption amount of the gas is the sum of the adsorption amounts of the layers. X-ray diffraction (XRD) experiments were carried out using a D/MX-IIIA diffractometer (Rigaku, Japan) to characterize the species distribution of the catalyst, crystallinity, and dispersivity of the supported species. Scanning electron microscopy (SEM) experiments were performed using the JSM-5610LV scanning electron microscope to determine the morphology and surface structure of the catalyst. X-ray photoelectron spectra (XPS) were carried out on a Thermo ESCALAB 250Xi apparatus with a monochromatic Al $K\alpha$ ($h\nu$ = 1486.6 eV) as the excitation source, to investigate the elemental states on the surface of the samples. All the binding energies were calibrated by the *C* 1s line at 284.6 eV Wang et al. [35].

3. Results and Discussion

3.1. Characterization of Samples

3.1.1. BET and XRD. The BET characterization results for different metal loading catalysts were shown in Table 1. The pure γ-Al_2O_3 has a relatively high specific surface area. The BET has a slight increase and then begins to decrease after Mn loading. This may be due to the small amount of load that causes γ-Al_2O_3 to adsorb on some tiny particles, which are beneficial to increase the specific surface area of the catalyst. When the Mn loading increases to a certain extent, the specific surface area will decrease. This may be because the metal occupies part of the pore space of γ-Al_2O_3, thereby causing clogging of the pores and agglomeration of the catalyst particles.

After loading Ce, the specific surface area, pore volume, and pore size of the catalyst change similarly to the loading of Mn. This may be because the thermal stability of cerium oxide is stronger. During the preparation process, especially during calcination, between cerium and manganese, the interaction can inhibit the agglomeration of manganese oxide.

In order to better compare the crystal composition of Mn-Ce-Al with Mn-Al and Mn-Ce-Cu-Al, the BET of $Mn_{0.1}Ce_{0.02}Cu_{0.03}Al$ was also shown in Table 1. The XRD diffraction pattern of $Mn_{0.1}$ Al, $Mn_{0.1}Ce_{0.02}Al$, $Mn_{0.1}Ce_{0.02}CuAl$ catalyst is shown in Figure 2. It can be seen from the figure that there are obvious γ-Al_2O_3 diffraction peaks at 36.3°, 46.4°, and 67.1°, and $Mn_{0.}1Ce_{0.02}Al$, $Mn_{0.1}Ce_{0.02}CuAl$

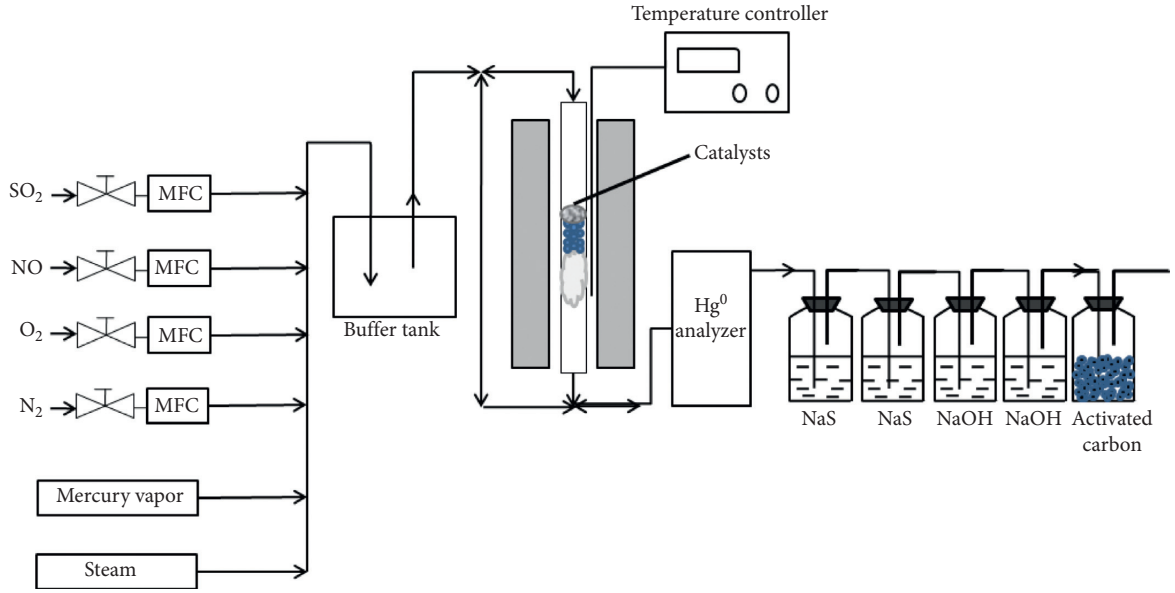

Figure 1: Schematic diagram of the experimental apparatus.

Table 1: BET characterization results for different metal loading catalysts.

Sample	BET (m^2/g)	Pore volume (cm^3/g)	Pore size (nm)
γ-Al_2O_3	242.71	0.416	6.55
$Mn_{0.03}$ Al	250.02	0.451	6.70
$Mn_{0.08}$ Al	243.32	0.420	6.58
$Mn_{0.1}$ Al	230.32	0.385	6.36
$Mn_{0.1}Ce_{0.01}Al$	232.11	0.390	6.38
$Mn_{0.1}Ce_{0.02}Al$	233.13	0.396	6.40
$Mn_{0.1}Ce_{0.05}Al$	229.13	0.385	6.33
$Mn_{0.1}Ce_{0.02}Cu_{0.03}Al$	227.47	0.388	6.35

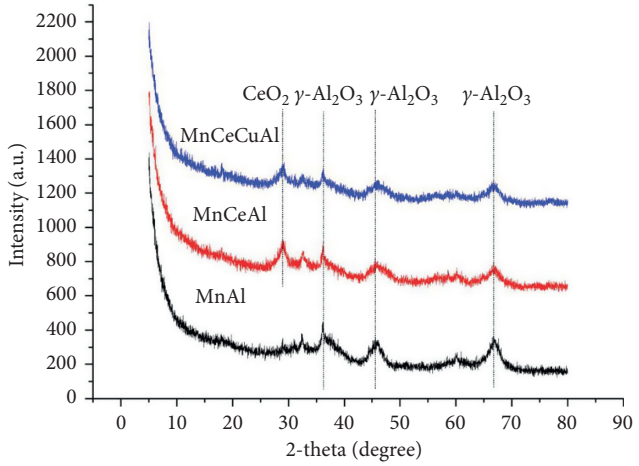

Figure 2: The XRD results of $Mn_{0.1}$ Al, $Mn_{0.1}Ce_{0.02}Al$, $Mn_{0.1}Ce_{0.02}CuAl$.

catalysts have a diffraction peak of 28.5°, but none of the three catalysts. A corresponding diffraction peak of Mn oxide (Mn_2O_3, MnO_2, etc.) was detected. This result can be explained by the single layer distribution theory [36]. When the amount of the supported substance is within a certain range, the surface of the carrier exists in a single layer distribution state. When the range is exceeded, the supported material will appear in the form of particles, and the characteristic diffraction peak characterized by XRD will be more obvious. Therefore, the diffraction peak of MnO_x which did not appear indicates that MnO_x did not undergo significant agglomeration and was uniformly distributed on the surface of the catalyst. At the same time, we observed that the peak intensity of γ-Al_2O_3 weakened after loading the active material, which also showed that the loading of the active metal increased the dispersibility of the surface material of the catalyst.

3.1.2. SEM. The figure below shows the SEM morphology of different magnifications of γ-Al_2O_3 and $Mn_{0.1}Ce_{0.02}Al$ catalysts. As shown in Figure 3, the pure γ-Al_2O_3 has an irregular crystal structure and a smooth surface. After loading Mn and Ce, the surface of the catalyst is covered with a layer of floc. The floc-like load is more conducive to increasing the contact area between the catalyst and the adsorbate, which has a certain promoting effect on the adsorption capacity of the catalyst.

3.1.3. XPS. The X-ray photoelectron spectroscopy analysis of Mn 2p before and after the mercury removal reaction of Mn-Ce/γ-Al_2O_3 catalyst through 1000 ppm SO_2 is shown in Figure 4(a). The characteristic peaks of Mn 2p are mainly Mn 2p3/2 and Mn 2p1/2, and the characteristic peaks of Mn 2p 3/2 can be fitted to three secondary peaks: Mn^{2+}, Mn^{3+}, and Mn^{4+}, and (1) the peak around 644.5 eV is Mn^{4+}. Characteristic peak, (2) the peak around 641.7 eV, is the characteristic peak of Mn^{3+} and (3) the peak around 641.4 eV is the characteristic peak of Mn^{2+} [37, 38]. It can be seen from the

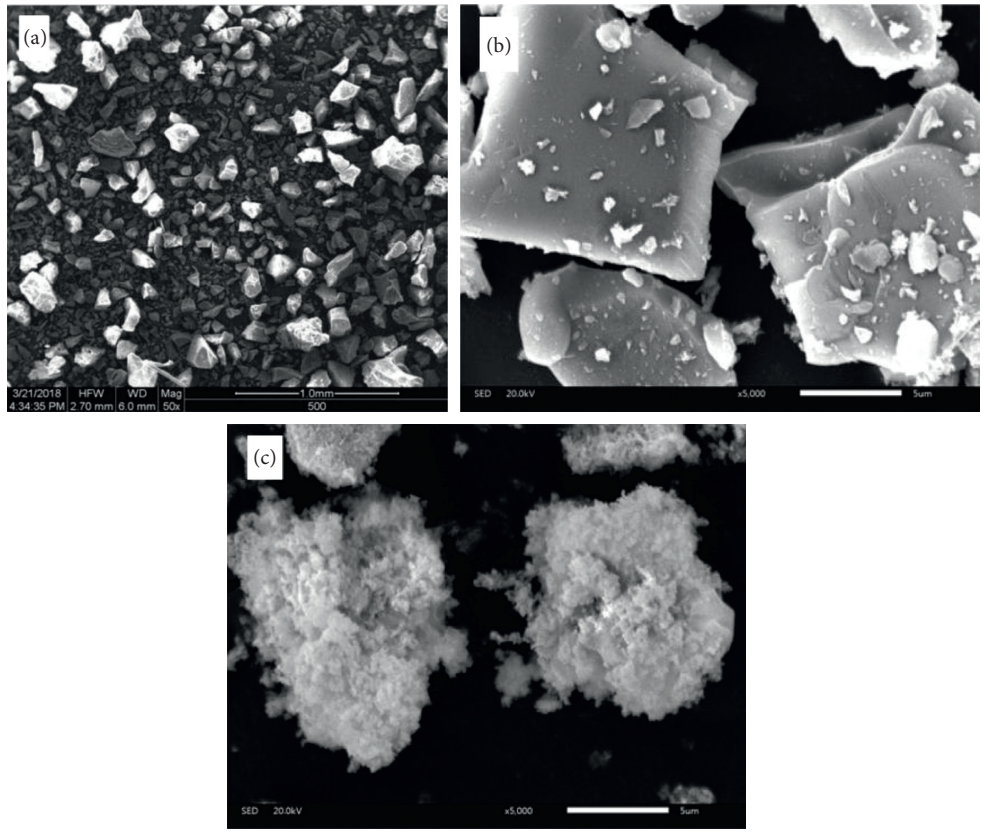

Figure 3: The SEM results of (a) γ-Al_2O_3-50; (b) γ-Al_2O_3-5000; (c) Mn-Ce/γ-Al_2O_3-5000.

figure that the form of Mn in the Mn-Ce/γ-Al_2O_3 composite oxide prepared by the coprecipitation method is mainly MnO_2 and Mn_2O_3, and MnO_2 accounts for more. The high characteristic ratio of Mn^{4+} is favorable for the oxidation of Hg^0 because Mn^{4+} has a stronger oxidation capacity than Mn^{3+} [39]. The good mercury removal ability of MnOx-CeOx/γ-Al_2O_3 composite oxide at low temperature is directly related to the high valence state of metal Mn.

After the mercury removal reaction, the ratio of Mn^{4+} characteristic peaks in Mn-Ce/γ-Al_2O_3 is low, and the characteristic peak of Mn^{2+} appears. This indicates that Mn-Ce/γ-Al_2O_3 has some Mn^{4+} in the catalytic oxidation of Hg^0 reduced to Mn^{3+} and Mn^{2+}.

As shown in Figure 4(a), we use u to represent the spin-orbital state of Ce 3d3/2 and v to represent the spin-orbital state of Ce 3d5/2 [39]. The u/v, $u2/v2$, and $u3/v3$ peak pair represents the $3d^{10}4f^0$ electronic state of Ce^{4+}, and the $u1/v1$ peak pair represents the $3d^{10}4f^1$ electronic state of Ce^{3+}. Previous studies have shown that there is no $u1/v1$ peak belonging to Ce^{3+} in the XPS spectrum of pure CeO_2 [24]. The synergistic effect of the support and manganese oxide in the catalyst can gradually increase the peak intensity of Ce^{3+}. The presence of Ce^{4+}/Ce^{3+} redox electron pairs on the catalyst surface can produce unbalanced charges, electron holes, and unsaturated chemical bonds [40]. These factors can enrich the surface of the catalyst with more chemically adsorbed oxygen, which is beneficial to the process. The conversion cycle between Ce^{4+} and Ce^{3+}, as well as the storage and release of oxygen on the surface of the composite oxide [41], thereby increases its ability to oxidize Hg^0. At the same time, after the catalytic oxidation of Mn-Ce/γ-Al_2O_3, the value of Ce^{4+}/Ce^{3+} decreased from 4.68 to 3.65. It can be concluded that, in the oxidation process of Hg^0, CeO_2 participates in the reaction and some Ce^{4+} converted to Ce^{3+}.

3.2. Determination of Mn and Ce Loading. The reaction results of MnO_x/Al_2O_3 catalysts with different loadings at $N_2 + 5\%O_2$ and a reaction temperature of 150°C are shown in Figure 5(a). The Hg^0 removal efficiency of pure γ-Al_2O_3 is only 8%, because it is mainly physical adsorption at this time. As the Mn loading increases, the Hg^0 removal efficiency is significantly improved. When the Mn/Al molar ratio is only 0.06, the Hg^0 removal efficiency increases to 40%, which shows that MnO_x and γ-Al_2O_3 have a chemical adsorption effect on the Hg^0 removal. When the Mn/Al molar ratio is 0.018, 0.03, 0.065, 0.08, and 0.1, Hg^0 removal efficiency gradually increases, corresponding to 65%, 73%, 78%, 80%, and 82%. However, when the Mn/Al molar ratio increases to 0.147, the Hg^0 removal efficiency did not increase to a great extent. When the Mn/Al molar ratio was 0.251, the Hg^0 removal efficiency even decreased. The excessive Mn doping will further block the pores and reduce the contact probability of Hg^0 and the active site. Besides, as Mn content increased, the crystallinity of MnOx on the support was

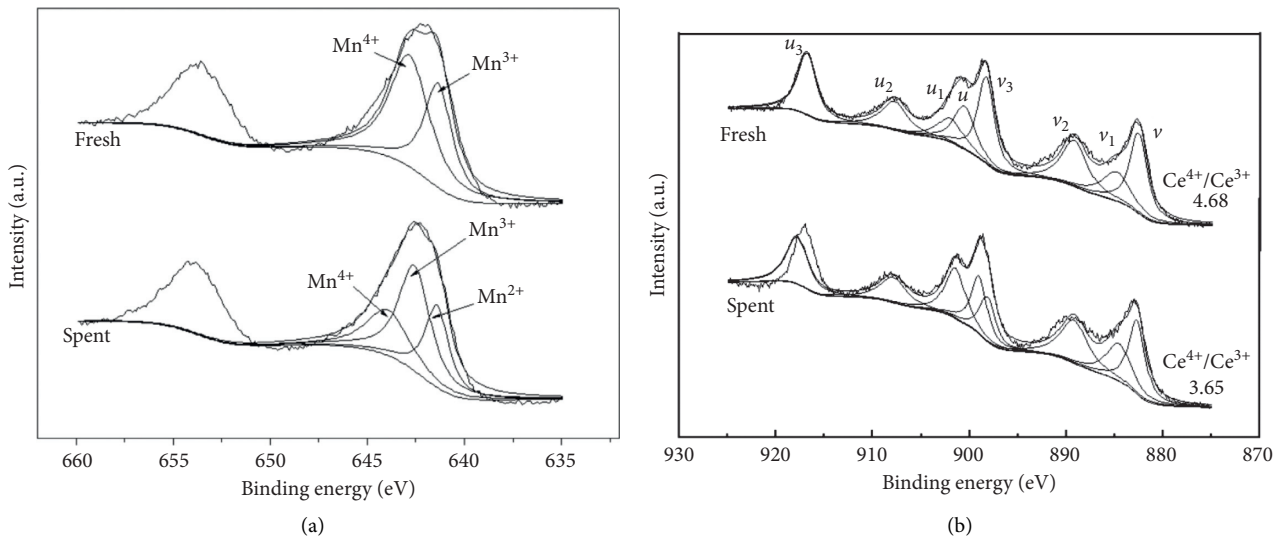

Figure 4: XPS spectra of: (a) fresh and spent catalysts for Mn 2p of Mn-Ce/γ-Al_2O_3; (b) fresh and spent catalysts for Ce 3d of Mn-Ce/γ-Al_2O_3.

enhanced, which was adverse for its catalytic performance [42], resulting in a slight decrease of the Hg^0 removal efficiency.

As shown in Figure 5(b), Mn remains the main active component of the adsorbent, but the doping of Ce can significantly increase the Hg^0 removal efficiency. When the molar ratio of Ce and Al is only 0.02, Hg^0 removal efficiency is closed to 93%. However, the Hg^0 removal efficiency has no significant change by continuing to increase the content of Ce.

Compared with pure γ-Al_2O_3, the Hg^0 removal efficiency may be increased for two reasons after loading the metal. First, CeO_2 can store or release oxygen atoms through the Ce^{4+}/Ce^{3+} redox electron pair and then pass through a series of the chemical reaction showing a strong catalytic effect, and as an important auxiliary component, it can also improve its oxidizing ability. Second, the incorporation of cerium can increase the specific surface area of the adsorbent, thereby increasing the mercury adsorption capacity of the adsorbent under low-temperature conditions, but excessive loading can cause clogging of the micropores, thereby reducing the physical and chemical adsorption capacity.

3.3. Effect of Calcination Temperature. During the preparation of the catalyst, the calcination temperature has an important influence on its activity. The mercury oxidation performance of the $Ce_{0.02}Mn_{0.1}Al$ catalyst is shown in Figure 6, the calcination temperature was 100, 200, 300, 400, 500, 600, 700, and 800°C, $N_2 + 5\%O_2$ flue gas condition, and the reaction temperature of mercury removal was 150°C. As the calcination temperature increases, the catalytic oxidation ability of the catalyst to mercury first increases and then decreases. When the catalyst was calcined at 100 to 400°C, the mercury removal efficiency increased. However, when the catalyst was calcined at 400 to 800°C, the mercury removal efficiency decreased rapidly, especially at high temperatures. The calcination temperature may affect the pore structure and surface crystal structure of the catalyst. The load component cannot be completely decomposed and converted into an active component at the low calcination temperature, and the supported component will occupy the surface of the carrier, thereby reducing the adsorption performance of the carrier. When the temperature rises, the active site will increase, and the oxidation efficiency will increase. However, when the temperature is higher than a certain value, the structure of the catalyst will be destroyed, and some active sites will be covered. At the same time, high temperature will make the active component sintered and the catalyst activity lowered. The optimal calcination temperature was 400°C, and the calcination temperature of the subsequent experimental catalyst was prepared at 400°C.

3.4. Effect of Reaction Temperature. To study the catalytic activity of the catalyst under low-temperature conditions, the Hg^0 removal rate in the range of 50°C to 250°C was conducted under the condition of N_2+5%O_2 flue gas using $Ce_{0.02}Mn_{0.1}Al$ catalyst. The results are shown in Figure 7.

It can be seen from the figure that the Hg^0 removal rate increases first and then decreases with the increase of temperature. When the reaction temperature is lower than 150°C, the removal efficiency of mercury increases with the increase of temperature, and the reaction temperature is higher than 150°C. The mercury removal efficiency decreases with increasing temperature. High activity is maintained between 100 and −200°C.

It has been revealed that Hg^0 oxidation over Mn-based catalyst follows the Mars–Maessen mechanism [42]. Hg^0 must adsorb onto the catalyst first and then be oxidized by the surface lattice oxygen to form HgO. Apparently, high

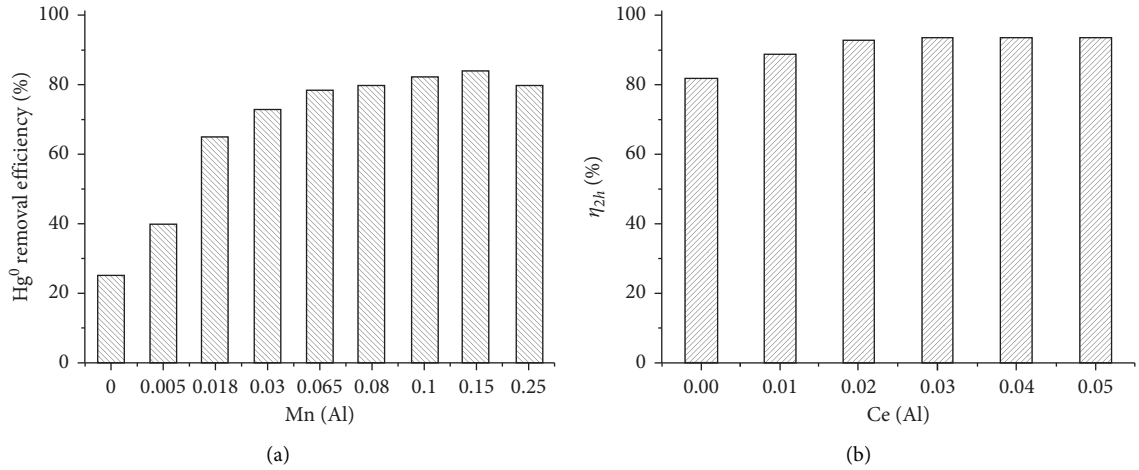

Figure 5: (a) Effect of Mn loading on Hg^0 removal efficiency; (b) effect of different Ce/Al ratios on catalytic oxidation of Hg^0.

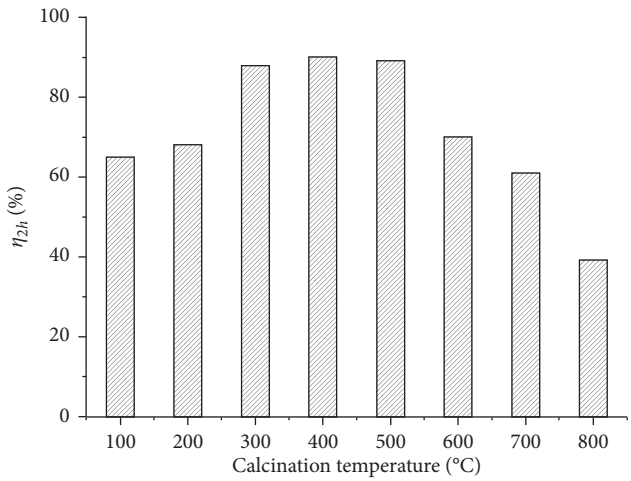

Figure 6: Effect of calcination temperature on catalytic oxidation of Hg^0.

temperature is not conducive to the effective physical adsorption of Hg^0 by the catalyst, resulting in lower Hg^0 removal efficiency. Low temperature was proper for the catalyst to remove Hg^0 [43, 44].

3.5. Effect of O_2. Figure 8 shows the change of Hg^0 removal efficiency under different O_2 concentration conditions of $Ce_{0.02}Mn_{0.1}Al$ type catalyst under N_2 as carrier gas and temperature of 150°C. It can be seen from the figure that O_2 plays an important role in the oxidation of Hg^0. When O_2 concentration increases from 0 to 5%, Hg^0 removal efficiency increases from 50% to 92%. When the O_2 concentration increases, the Hg^0 removal efficiency will be slight and decline. It is known that the O_2 concentration in the flue gas is about 4.5%. Therefore, the O_2 concentration under the conventional coal-fired flue gas condition can satisfy the effective oxidation of Hg^0.

3.6. Effect of SO_2. The SO_2 in the flue gas has a great influence on the activity of the catalyst, which may cause the passivation of the catalyst to be deactivated [45, 46]. The catalyst is intended to catalyze the oxidation of Hg^0 before the desulphurization system. Therefore, it is necessary to study the mercury removal performance of the catalyst under a high concentration of SO_2. Figure 9 shows the Hg^0 removal rate at a temperature of 150°C under a condition of $N_2 + 5\%$ O_2 flue gas using a $Ce_{0.02}$ Mn $_{0.1}$ Al type catalyst.

It can be seen from the figure that, with the increase of SO_2 concentration, the mercury removal efficiency gradually decreases. When the SO_2 concentration is 2000 ppm, the mercury removal rate is only 50%, which indicates that the presence of SO_2 will greatly inhibit the catalytic oxidation of Hg^0. This may be due to the competitive adsorption of SO_2 and Hg^0 on the surface of the catalyst under N_2 conditions; that is, SO_2 reacts with the active oxygen on the surface of the catalyst to form SO_3 [6], thereby reducing the reaction rate of Hg^0 with the surface active oxygen of the catalyst. In addition, SO_2 may react with MnO_x to form a stable $MnSO_4$, covering the surface of the catalyst, causing poisoning of the catalyst.

3.7. Mechanism. Through the above reaction results and characterization, the catalytic oxidation of Mn-Ce/γ-Al_2O_3 to mercury in the absence of HCl can be explained by the Mars–Maessen mechanism [21]. The following are specific reactions:

$$Hg^0(g) \longrightarrow Hg^0(ads) \quad (1)$$

$$Hg^0(ads) + MnO_x \longrightarrow Hg - O - Mn - O_{x-1} \quad (2)$$

$$Hg - O - Mn - O_{x-1} \longrightarrow HgO(ads) + MnO_{x-1} \quad (3)$$

$$Mn - O_{x-1} + \frac{1}{2}O_2 \longrightarrow MnO_x \quad (4)$$

To verify the above conjecture, experiments on the change of mercury removal efficiency of MnO_x-CeO_x/γ-Al_2O_3 at different temperatures and different times under anaerobic and aerobic conditions were carried out. It can be seen from Figure 10 that, under pure N_2 conditions, the

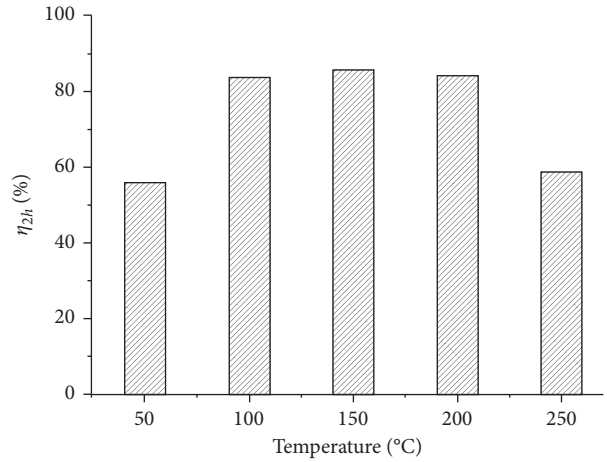

Figure 7: Effect of reaction temperature on catalytic oxidation of Hg^0.

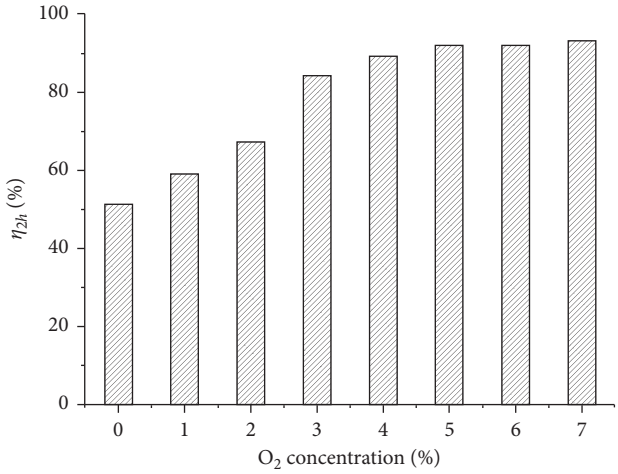

Figure 8: Effect of O_2 on catalytic oxidation of Hg^0.

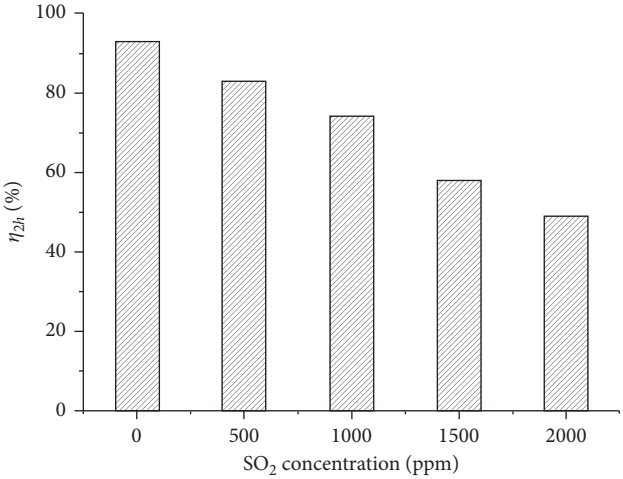

Figure 9: Effect of SO_2 on catalytic oxidation of Hg^0.

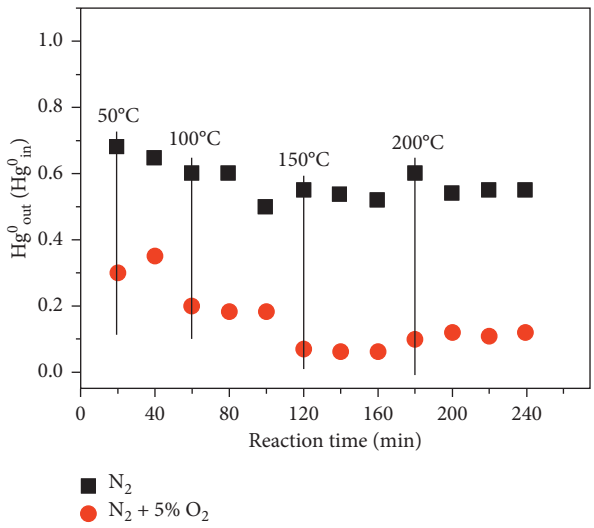

FIGURE 10: Experimental study on reaction mechanism of MnOx-CeOx/γ-Al_2O_3 catalyst.

oxidative removal efficiency of mercury is up to about 48%, while the γ-Al_2O_3 with a higher specific surface area is only 25% under the same conditions, which indicates that, under anaerobic conditions, lattice oxygen may participate in the reaction. When 5% O_2 was added to N_2, the mercury removal efficiency was improved as a whole. When the reaction was carried out at 150°C for 140 min, the mercury oxidative removal efficiency reached 93%, indicating that the newly added O_2 promoted the lattice oxygen to continue to function. Thereby, more Hg^0 is oxidized.

Meanwhile, as shown in Figure 10, when the reaction temperature is increased to 200°C, even if the reaction time is increased, the mercury oxidative removal efficiency is lowered, which indicates that Hg^0 formed on the catalyst is released or unstable due to higher temperature.

4. Conclusions

γ-Al_2O_3 supports the active components Mn and Ce, which greatly improves the catalytic oxidation performance of Hg^0. The catalyst (molar ratio) of $Mn_{0.1}Ce_{0.02}Al$ has the best activity, and the optimum calcination temperature for the preparation of the catalyst is 400°C. The optimal activity temperature ranges of the Mn-Ce/γ-Al_2O_3 catalyst are 100–200°C. Under the condition of lower reaction temperature, Hg^0 can be effectively removed, and the Hg^0 emission standard is increasingly strict. It is a simple and effective means of mercury removal. The SO_2 in the flue gas forms competitive adsorption on the catalyst, which leads to a decrease in the efficiency of the Hg^0 oxidation reaction at the active site and inhibits the mercury removal activity of the catalyst.

Data Availability

The data used to support the findings of this study are included within the article.

Conflicts of Interest

The authors declare that they have no conflicts of interest.

Acknowledgments

The authors would like to thank Test Center of Wuhan University for the support.

References

[1] W. Zhen, M. M. L, and H. T. Guo, "A strategic path for the goal of clean-and-low-carbon energy in China," *Natural Gas Industry B*, vol. 3, p. 4, 2017.

[2] N. Pirrone, S. Cinnirella, X. Feng et al., "Global mercury emissions to the atmosphere from natural and anthropogenic sources," in *Mercury Fate and Transport in the Global Atmosphere*, pp. 1–47, Springer US, New York, NY, USA, 2009.

[3] J. H. Pavlish, E. A. Sondreal, M. D. Mann et al., "Status review of mercury control options for coal-fired power plants," *Fuel Processing Technology*, vol. 82, no. 2-3, pp. 89–165, 2003.

[4] J. Wilcox, E. Rupp, S. C. Ying et al., "Mercury adsorption and oxidation in coal combustion and gasification processes," *International Journal of Coal Geology*, vol. 90-91, pp. 4–20, 2012.

[5] A. A. Presto and E. J. Granite, "Survey of catalysts for oxidation of mercury in flue gas," *Environmental Science & Technology*, vol. 40, no. 18, pp. 5601–5609, 2006.

[6] E. ChangDene and J. Wilcox, "Mercury species and SO_2 adsorption on CaO (100)," *The Journal of Physical Chemistry C*, vol. 112, no. 42, pp. 16484–16490, 2008.

[7] L. Ji, P. M. Sreekanth, P. G. Smirniotis, S. W. Thiel, and N. G. Pinto, "Manganese oxide/titania materials for removal of NO_x and elemental mercury from flue gas," *Energy & Fuels*, vol. 22, no. 4, pp. 2299–2306, 2008.

[8] S. Qiao, J. Chen, J. Li et al., "Adsorption and catalytic oxidation of gaseous elemental mercury in flue gas over MnO_x/alumina," *Industrial & Engineering Chemistry Research*, vol. 48, no. 7, pp. 3317–3322, 2009.

[9] J. A. Hrdlicka, W. S. Seames, M. D. Mann, D. S. Muggli, and C. A. Horabik, "Mercury oxidation in flue gas using gold and palladium catalysts on fabric filters," *Environmental Science & Technology*, vol. 42, no. 17, pp. 6677–6682, 2008.

[10] Y. Zhuang, J. Laumb, R. Liggett, M. Holmes, and J. Pavlish, "Impacts of acid gases on mercury oxidation across SCR catalyst," *Fuel Processing Technology*, vol. 88, no. 10, pp. 929–934, 2007.

[11] T. J. Feeley, L. A. Brickett, and A. O'Palko, *Mercury R&D Program Review*, US DOE, Washington, DC, USA, 2005.

[12] J. Li, N. Yan, Z. Qu et al., "Catalytic oxidation of elemental mercury over the modified catalyst Mn/α-Al_2O_3 at lower temperatures," *Environmental Science & Technology*, vol. 44, no. 1, pp. 426–431, 2010.

[13] Z. S. Wei, Y. W. Luo, B. R. Li et al., "Elemental mercury oxidation from flue gas by microwave catalytic oxidation over Mn/$_\gamma$-Al_2O_3," *Journal of Industrial and Engineering Chemistry*, vol. 24, pp. 315–321, 2015.

[14] X. Wen, C. Li, X. Fan et al., "Experimental study of gaseous elemental mercury removal with CeO_2/γ-Al_2O_3," *Energy & Fuels*, vol. 25, no. 7, pp. 2939–2944, 2011.

[15] Y. Xie, C. Li, L. Zhao et al., "Experimental study on Hg^0 removal from flue gas over columnar MnO_x-CeO_2/activated coke," *Applied Surface Science*, vol. 333, pp. 59–67, 2015.

[16] W. Xu, H. Wang, X. Zhou, and T. Zhu, "CuO/TiO_2 catalysts for gas-phase Hg^0 catalytic oxidation," *Chemical Engineering Journal*, vol. 243, pp. 380–385, 2014.

[17] A. Yamaguchi, H. Akiho, and S. Ito, "Mercury oxidation by copper oxides in combustion flue gases," *Powder Technology*, vol. 180, no. 1-2, pp. 222–226, 2008.

[18] W. Yang, Y. Liu, Q. Wang, and J. Pan, "Removal of elemental mercury from flue gas using wheat straw chars modified by Mn-Ce mixed oxides with ultrasonic-assisted impregnation," *Chemical Engineering Journal*, vol. 326, pp. 169–181, 2017.

[19] B. Zhao, X. Liu, Z. Zhou, H. Shao, and M. Xu, "Catalytic oxidation of elemental mercury by Mn-Mo/CNT at low temperature," *Chemical Engineering Journal*, vol. 284, pp. 1233–1241, 2016.

[20] B. Zhao, H. Yi, X. Tang, Q. Li, D. Liu, and F. Gao, "Copper modified activated coke for mercury removal from coal-fired flue gas," *Chemical Engineering Journal*, vol. 286, pp. 585–593, 2016.

[21] E. J. Granite, H. W. Pennline, and R. A. Hargis, "Novel sorbents for mercury removal from flue gas," *Industrial & Engineering Chemistry Research*, vol. 39, no. 4, pp. 1020–1029, 2000.

[22] X. Thornton, C. Li, G. Zeng et al., "Removal of gas-phase element mercury by activated carbon fiber impregnated with CeO_2," *Energy & Fuels*, vol. 24, no. 8, pp. 4250–4254, 2010.

[23] L. Tian, C. Li, Q. Li, G. Zeng, Z. Gao, and S. X. Li, "Removal of elemental mercury by activated carbon impregnated with CeO_2," *Fuel*, vol. 88, no. 9, pp. 1687–1691, 2009.

[24] J. He, G. K. Reddy, S. W. Thiel, P. G. Smirniotis, and N. G. Pinto, "Ceria-modified manganese oxide/titania materials for removal of elemental and oxidized mercury from flue gas," *The Journal of Physical Chemistry C*, vol. 115, no. 49, pp. 24300–24309, 2011.

[25] J. An, J. Lou, Q. Meng, Z. Zhang, X. Ma, and J. Li, "Non-thermal plasma injection-CeO_2-WO_3/TiO_2 catalytic method for high-efficiency oxidation of elemental mercury in coal-fired flue gas," *Chemical Engineering Journal*, vol. 325, pp. 708–714, 2017.

[26] H. Li, S. Wu, C.-Y. Wu, J. Wang, L. Li, and K. Shih, "SCR atmosphere induced reduction of oxidized mercury over CuO-CeO_2/TiO_2 catalyst," *Environmental Science & Technology*, vol. 49, no. 12, pp. 7373–7379, 2015.

[27] Z. Li, Y. Shen, X. Li, S. Zhu, and M. Hu, "Synergetic catalytic removal of Hg^0 and NO over $CeO_2(ZrO_2)/TiO_2$," *Catalysis Communications*, vol. 82, pp. 55–60, 2016.

[28] L. Zhao, C. Li, S. Li et al., "Simultaneous removal of elemental mercury and NO in simulated flue gas over V_2O_5/ZrO_2-CeO_2 catalyst," *Applied Catalysis B: Environmental*, vol. 198, pp. 420–430, 2016.

[29] B. Li, Z. Ren, Z. Ma et al., "Selective catalytic reduction of NO by NH_3 over CuO-CeO_2 in the presence of SO_2," *Catalysis Science & Technology*, vol. 6, no. 6, pp. 1719–1725, 2016.

[30] H. Li, C.-Y. Wu, Y. Li, and J. Zhang, "Superior activity of $MnOx$-CeO_2/TiO_2 catalyst for catalytic oxidation of elemental mercury at low flue gas temperatures," *Applied Catalysis B: Environmental*, vol. 111-112, pp. 381–388, 2012.

[31] P. Fan, S. Su, J. Xiang et al., "Catalytic oxidation of Hg^0 by MnO_x-CeO_2/γ-Al_2O_3 catalyst at low temperatures," *Chemosphere*, vol. 101, pp. 49–54, 2014.

[32] H. Li, S. Wang, X. Wang, N. Tang, S. Pan, and J. Hu, "Catalytic oxidation of Hg^0 in flue gas over Ce modified TiO_2 supported Co-Mn catalysts: characterization, the effect of gas composition and co-benefit of NO conversion," *Fuel*, vol. 202, pp. 470–482, 2017.

[33] H. Li, Y. Wang, S. Wang, X. Wang, and J. Hu, "Removal of elemental mercury in flue gas at lower temperatures over Mn-Ce based materials prepared by co-precipitation," *Fuel*, vol. 208, pp. 576–586, 2017.

[34] H. H. Li, J. J. Hu, and H. Wang, "Catalytic oxidation removal of elemental mercury in flue gas over niobium-loaded catalyst," *Canadian Journal of Chemical Engineering*, vol. 94, pp. 1486–1494, 2016.

[35] Y. Wang, H. Li, S. Wang, X. Wang, Z. He, and J. Hu, "Investigation of sulphated $CuCl_2/TiO_2$ catalyst for simultaneous removal of Hg^0 and NO in SCR process," *Fuel Processing Technology*, vol. 188, pp. 179–189, 2019.

[36] Y.-C. Xie and Y.-Q. Tang, "ChemInform abstract: spontaneous monolayer dispersion of oxides and salts onto surfaces of supports: applications to heterogeneous catalysis," *ChemInform*, vol. 22, no. 41, 1990.

[37] C. He, B. Shen, J. Chen, and J. Cai, "Adsorption and oxidation of elemental mercury over Ce-MnO_x/Ti-PILCs," *Environmental Science & Technology*, vol. 48, no. 14, pp. 7891–7898, 2014.

[38] X. Lu, C. Song, S. Jia, Z. Tong, X. Tang, and Y. Teng, "Low-temperature selective catalytic reduction of NO_X with NH_3 over cerium and manganese oxides supported on TiO_2-graphene," *Chemical Engineering Journal*, vol. 260, pp. 776–784, 2015.

[39] P. Burroughs, A. Hamnett, and A. F. Orchard, "Satellite structure in the X-ray photoelectron spectra of some binary and mixed oxides of lanthanum and cerium," *Journal of the Chemical Society, Dalton Transactions*, vol. 17, no. 17, pp. 1686–1698, 1976.

[40] X. Gao, Y. Jiang, Y. Zhong, Z. Luo, and K. Cen, "The activity and characterization of CeO_2-TiO_2 catalysts prepared by the sol-gel method for selective catalytic reduction of NO with NH_3," *Journal of Hazardous Materials*, vol. 174, no. 1–3, pp. 734–739, 2010.

[41] Z. Huang, Z. Zhu, and Z. Liu, "Combined effect of H_2O and SO_2 on V_2O5/AC catalysts for NO reduction with ammonia at lower temperatures," *Applied Catalysis B: Environmental*, vol. 39, no. 4, pp. 361–368, 2002.

[42] S. Zhang, Y. Zhao, Z. Wang, J. Zhang, L. Wang, and C. Zheng, "Integrated removal of NO and mercury from coal combustion flue gas using manganese oxides supported on TiO_2," *Journal of Environmental Sciences*, vol. 53, pp. 141–150, 2017.

[43] S. Zhang, Y. Zhao, J. Yang et al., "Simultaneous NO and mercury removal over MnO_x/TiO_2 catalyst in different atmospheres," *Fuel Processing Technology*, vol. 166, pp. 282–290, 2017.

[44] S. Zhang, Y. Zhao, J. Yang, J. Zhang, and C. Zheng, "Fe-modified MnO_x/TiO_2 as the SCR catalyst for simultaneous removal of NO and mercury from coal combustion flue gas," *Chemical Engineering Journal*, vol. 348, pp. 618–629, 2018.

[45] C. W. Lee, R. K. Srivastava, S. B. Ghorishi, T. W. Hastings, and F. M. Stevens, "Investigation of selective catalytic reduction impact on mercury speciation under simulated NO_x emission control conditions," *Journal of the Air & Waste Management Association*, vol. 54, no. 12, pp. 1560–1566, 2004.

[46] C. Richardson, T. Machalek, S. Miller, C. Dene, and R. Chang, "Effect of NO_x control processes on mercury speciation in utility flue gas," *Journal of the Air & Waste Management Association*, vol. 52, no. 8, pp. 941–947, 2002.

[47] X.-Y. Hua, J.-S. Zhou, Q. Li, Z.-Y. Luo, and K.-F. Cen, "Gas-phase elemental mercury removal by CeO_2 impregnated activated coke," *Energy & Fuels*, vol. 24, no. 10, pp. 5426–5431, 2010.

[48] S. Yang, Y. Guo, N. Yan et al., "Remarkable effect of the incorporation of titanium on the catalytic activity and SO_2 poisoning resistance of magnetic Mn-Fe spinel for elemental mercury capture," *Applied Catalysis B: Environmental*, vol. 101, no. 3-4, pp. 698–708, 2011.